IEEE Robotics and Automation Letters (RAL) paper presented at the
2020 IEEE/RSJ International Conference on Intelligent Robots and Systems (IROS)
October 25-29, 2020, Las Vegas, NV, USA (Virtual)

BLT Gripper: An Adaptive Gripper with Active Transition Capability between Precise Pinch and Compliant Grasp*

Yong-Jae Kim,[1] *Member, IEEE*, Hansol Song[2], and Chan-Young Maeng[3]

***Abstract*— Achieving both the precise pinching and compliant grasping capabilities is a challenging goal for most robotic hands and grippers. Moreover, an active transition between the pinching pose and the grasping pose is difficult for limited degrees-of-freedom (DOF) hands or grippers. Even when using high DOF robotic hands, it requires a substantial amount of control effort and information from tactile sensors. In this paper, a 3-finger, 5-DOF adaptive gripper with active transition capability is presented. Each finger is composed of a minimum number of components using one rigid link, one belt, one fingertip frame and one motor for flexion motion. This simple and unique finger structure enables precise parallel pinching and highly compliant stable grasping with evenly distributed pressure. The other two motors are used for fingertip angle adjustment and change of the finger orientation respectively. Thorough kinematic and force analysis with detailed descriptions of the mechanical design clearly shows controllable transition property and stable grasping performance. The experiments including the grasping force and pressure measurement verify the performance of the proposed gripper and prove the practical usefulness for real-world applications.**

I. INTRODUCTION

In real-world situations, utilizing tools to accomplish a task often requires a large variety of grasp types. For instance, in order to use a small screwdriver, the user pinches the handle using 2 or 3 fingertips and changes to a compliant grasping pose to apply high torque. After using it, the user returns to the pinch pose to lay it down gently on the table. This simple example not only requires the extreme types of grasping - precise pinching and compliant grasping - but also the smooth and stable transition between the grasping modes.

To categorize and utilize the functions of the human hand, many studies on grasping taxonomies have been investigated [1][2]. These studies identify greater than 20 or 30 distinctive grasp types, which implies the versatility of the human hand. To realize similar capability, various types of high degrees-of-freedom (DOF) human-like robotic hands have been developed [3][4][5] aiming at the performance of a human hand having 15 joints and more than 20 DOFs. They contain complex and expensive mechanisms and sensors and require complicated motion planning and control, all which hinders their widespread use in practical applications and further commercialization.

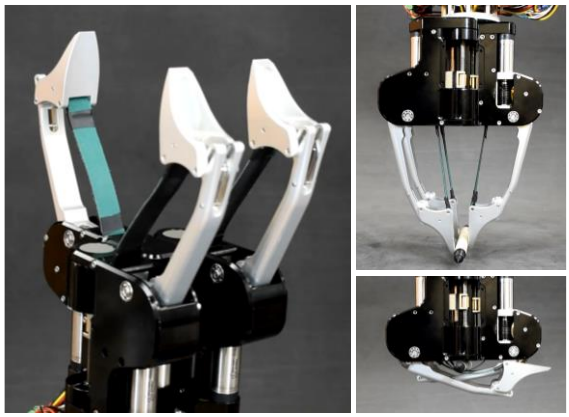

Fig. 1. Proposed BLT Gripper (Belt and Link actuated Transformable adaptive Gripper with active transition capability).

Based on the grasp taxonomy in [1], grasping can be categorized into precision grasps and power grasps. One of the important grasp modes in the precision grasp is pinching objects with parallel fingertip surfaces, which will be referred to as parallel pinching in this paper. One of the important aspects of the power grasp is adaptability to irregularly shaped objects. Therefore, the power grasp focusing on compliance to the arbitrary shapes will be referred to as compliant grasping in this paper. Focusing on compliant grasping capability with reduced mechanical complexity and a fewer number of actuators, various approaches including under-actuated mechanisms [6], synergy based mechanisms [7], and soft and flexible mechanisms [8] are being continuously investigated. Their inherent adaptability to arbitrarily shaped objects enables simplified control strategy and safe interaction with objects and environment. The iHY Hand [9] and Yale OpenHand [10], which utilize under-actuated monolithic finger structures, showed remarkable robustness and adaptability with relatively simple mechanisms. Nonetheless, this inherent compliance may reduce the abilities of precise manipulation and the ability to change the grasping mode. To overcome these, many control schemes such as the extrinsic dexterity which actively utilizes the environment and gravity [11] and adoption of human finger motions [12] are being studied. Various novel mechanisms have been introduced to increase the performance of under-actuated hands. For instance, the Velvet Fingers utilizes conveyor systems as active contact surfaces to achieve in-hand object rotation and translation capability [13]. Another example is the use of deformable rubber bags filled with fluid to enhance grasping capabilities with various grasping modes [14].

*Resrach supported by NAVER Labs. Co.

[1].Yong-Jae Kim, is with Korea University of Technology and Education (Koreatech), Cheonan-City, Rep. of Korea (corresponding author to provide phone: +82-41-560-1424; fax: +82-41-564-3261; e-mail: yongjae@koreatech.ac.kr).

[2]Hansol Song and [3]Chan-Young Maeng are with Korea University of Technology and Education (Koreatech), Cheonan-City, Rep. of Korea (e-mail: stan44@koreatech.ac.kr, aodrnrj@koreatech.ac.kr).

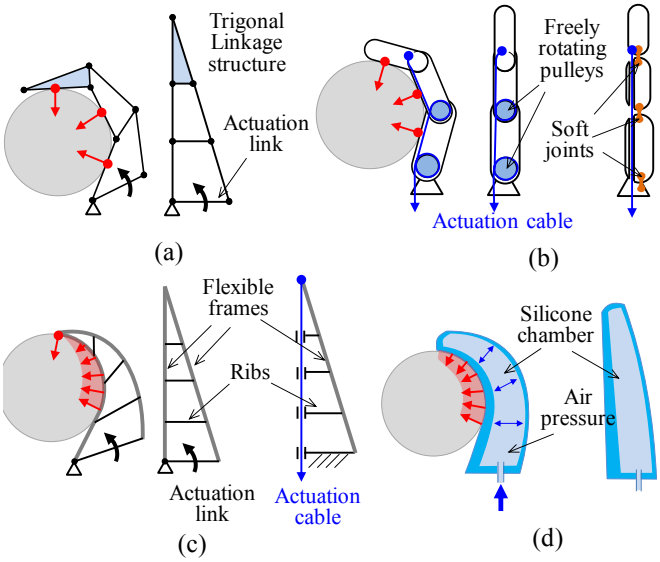

Fig. 2. Conceptual examples of adaptive grasping. (a) An under-actuated finger composed of multiple trapezoidal 4-bars. (b) An under-actuated finger using joints and tendons. (c) Complaint finger mechanisms using flexible structures and flexures. (d) A soft finger actuated by air pressure.

To achieve both precise pinching and compliant grasping capability through mechanical design, several universal grippers have been proposed. The Sarah hand [6] and its commercial product Robotiq 3-Finger Gripper [15] have the combined structure of under-actuated mechanism for the compliant grasping and the parallelogram linkage for the precise parallel pinch. The Robotiq Adaptive Gripper [16], widely used in research field recently, has an elegant mechanism to realize the two grasping modes with a significantly simpler mechanism. The detailed explanation is provided in Section II. These two grasping modes also can be accomplished by using coupling tendons and actuation tendons as implemented in the Velo gripper [17]. The ParaGripper composed of multiple parallel 4-bar links and parallel fingertips also achieved both the parallel pinching and power grasp as well as in-hand manipulation capability [18]. Although the active transition between the different grasping modes is also a critical issue as aforementioned, these grippers do not provide active transition ability. Thus, finding the proper gripper mechanisms which provide various grasping modes enabling stable and active transition between the modes is still to be further explored.

As an effort of this, this paper proposes a 3-finger 5-DOF robotic gripper with an active transition capability as shown in Fig.1. Each finger is composed of a minimum number of components; one rigid actuation link, one belt, one fingertip frame, and one motor. The simple and unique finger structure enables precise parallel pinching and highly complaint stable grasping with evenly distributed pressure. The remainder of this paper is organized as follows. Section II introduces the concept of adaptive grippers and the idea of the proposed gripper. In Section III, kinematic analysis and the force distribution analysis are described. In Section IV, the detail design and implementation are presented. Section V presents the experimental reports the evaluation results, and Section VI provides conclusion and future work.

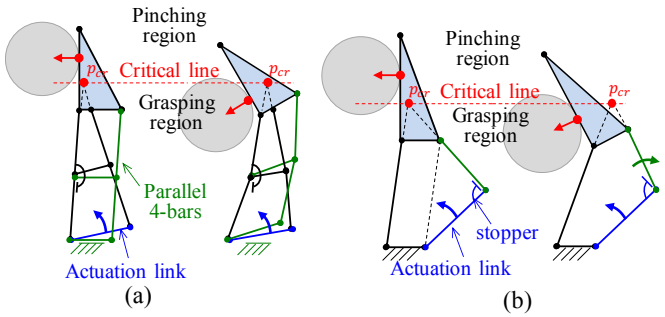

Fig. 3. Combined structures having parallel pinch and compliant grasp. (a) Sarah hand [6]. (b) Robotiq Adaptive Gripper [16].

II. Basic Concept of Adaptive Grippers

A. Concept of Adaptive Grasping Mechanisms

Fig.2 (a) and (b) illustrate the representative examples of under-actuated finger mechanisms. The triangular linkage structure in Fig.2 (a), a simplified illustration of the under-actuated finger in [6], has 3 DOFs and 1 actuation. When the actuation link at the bottom rotates, the structure conforms to the object and produces distributed contact forces. This linkage structure is suitable for high payload grasping, but it may reduce the range of motion. Fig.2 (b) shows a similar under-actuated mechanism but with a more human-like mechanism using tendons. The tendons goes around the free-rotating pulleys (blue circles) centered at the revolute joints and the tension of the tendon produces a constant torque distribution to all joint. This torque distribution to each joint is clearly determined by the radius of the pulleys [19]. For simplicity and more compliance, the revolute joint can be replaced with a flexure and the tendon routing can be simplified as shown in the right most figure of Fig. 2(b) [9][10][12]. Another approach is to utilize the material flexibility. Fig. 2(c) shows the well-known Fin-Gripper from FESTO Co. which comprises 2 flexible frames and multiple ribs [20]. It continuously wraps around the object and applies a well-distributed pressure rather than point contacts, which provides more stable and safe grasping. There are many mechanisms with similar concepts [21][22]. For more compliance and safely, soft materials and air pressure can be used as shown in Fig. 2(d). The tradeoff for these advantages can be a sacrifice in precision of the grasping position and a lower payload. The ideal goal for compliant grasping is to provide uniform force or pressure regardless of the object size and shape.

B. Principles of the Transition between the Parallel Pinch and Compliant Grasp

By combining the under-actuated structure of Fig. 2(a) and parallel 4-bar linkages, both the complaint grasping and parallel pinching can be achieved as shown in Fig. 3(a), where the green colored links represent the parallel 4-bar linkages. The behavior depends on the position of contact point in relation to the p_{cr} which is the intersection of point of the two extended lines of the vertical links of the triangular linkage (black colored links). If the contact with the object occurs above the intersection point p_{cr}, the fingertip maintains the

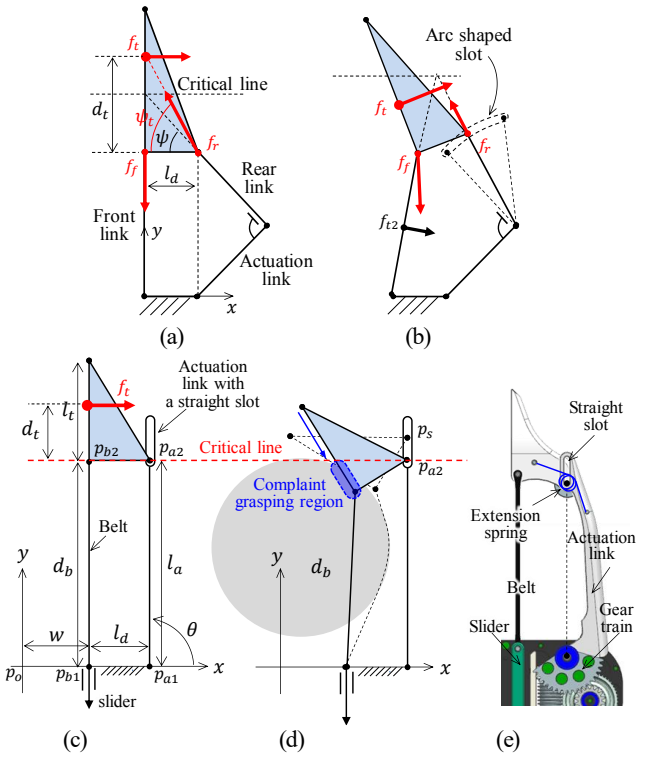

Fig. 4. (a) and (b) Free body diagrams of the fingertip of the Robotiq Adaptive Gripper. (c) and (d) Proposed finger mechanism. (e) Mechanical design of the proposed finger.

vertical pose by the support of the parallel 4-bars. Otherwise, if the contact occurs lower than p_{cr}, the triangular linkage starts grasping the object. Therefore, the horizontal line containing p_{cr}, named the critical line, determines the pinching region and grasping region. For further explanation, refer to [6].

The Robotiq Adaptive Gripper achieves similar capability with a significantly simpler mechanism. Basically, it acts as a parallel 4-bar mechanism as shown in the left figure of Fig. 3(b), but the right vertical link is composed of two links with a stopper (green and blue links). Similarly, the intersection point p_{cr} of the extended lines of the black and green links determines the critical line. When the contact occurs above the line, the stopper remain compressed and the mechanism works as a parallel 4-bar. Otherwise, the stopper detaches and the finger will start to bend to grasp the object as illustrated in the rightmost figure of Fig. 3(b).

These two mechanisms accomplish the parallel pinching and compliant grasping without increasing the number of actuators. However, the grasping type is determined only by the contact region, which means that once the grasping type is determined it cannot be actively changed. Moreover, there are practical issues. The mass of the passively moving parts, i.e. the fingertip, the black link, and the green link in Fig. 3(b) can cause undesirable vibration when the gripper is moving while mounted on a manipulator. Also, more distributed contact forces or contact pressure are required for more stable grasping.

C. Basic Concept of the Proposed BLT Gripper

The analysis of the Robotiq Adaptive Gripper yields useful intuition of adaptive gripping mechanics. Fig. 4(a) shows the parallel pinching pose, where l_d, d_t, and ψ denote the length of the bottom link of the 4-bar, the distance between the bottom line of the fingertip and the contact point, and the angle between the rear link and the x-axis. When the actuation link is fixed by the actuators, the fingertip receives 3 forces f_t, f_f, and f_r, which indicate the contact force, the tensile force from the front link, and the compressive force from the rear link, respectively. ψ_t indicates the direction of force f_r. From the free-body diagram of the fingertip, the force and moment equilibrium equations can be obtained as

$$\begin{aligned} \Sigma F_x: \quad & f_t - f_r \cos\psi_t = 0, \\ \Sigma F_y: \quad & f_f - f_r \sin\psi_t = 0, \\ \Sigma M: \quad & f_f\, l_d - f_t\, d_t = 0. \end{aligned} \tag{1}$$

From (1), ψ_t direction of f_r has following relationship as

$$\tan\psi_t = d_t \,/\, l_d \tag{2}$$

which means that force vector of f_r is on the line between the contact point and the distal joint of the rear link. In the case of $\psi_t > \psi$, where the contact point is above the critical line as shown in Fig. 4(a), the rear link is in contact with the actuation link via the stopper and the finger maintains a parallel pose. On the other hand, if $\psi_t < \psi$, where the contact point is under the critical line as shown in Fig. 4(b), the distal joint of the rear link moves along an arc-shaped path and the finger starts to grasp the object compliantly. From the behavior of the Robotiq gripper, we can find that the role of the rear link is guiding the fingertip along an arc-shaped curve, and therefore the rear link can be replaced with a slot. Another notable fact is that the front link always receives tensile force. A flexible belt can substitute for the front link and may increase the even distribution of contact forces.

Considering the above analysis, a new finger mechanism is proposed as shown in Fig. 4(c). The front link and the rear link were replaced by a belt and a slot respectively. In order to secure the large parallel pinching region when pinching objects and to make the mechanism simple, the slot was designed to have a straight shape along the actuation link. Instead, to actively transit to the compliant grasping mode, a slider adjusting the belt length was added. As shown in Fig. 4(d), by reducing the belt length, the fingertip closes around the object and the contact point moves to the compliant grasping region (blue area). Then, the finger compliantly grasps the object. Fig. 4(e) shows its mechanical design. The actual actuation link was designed as a curved shape to avoid contact with the belt when grasping small objects. To keep the fingertip straight when not in contact, a spring is placed between the fingertip and the actuation link. As the passively moving parts are only the lightweight belt and the fingertip, it does not cause unwanted vibration when moving on a manipulator.

III. Kinematics and Force Distribution

A. Kinematics at the Compliant Grasping Pose

Let us assume that the finger is grasping a circular object as shown in Fig. 5(a). In most cases, contact occurs in three areas: the fingertip, the belt and the palm. As indicated in Fig. 4(c) (also in Fig. 5(a)), the points p_o, p_{b1}, p_{b2}, p_{a1}, p_{a2}, and p_t

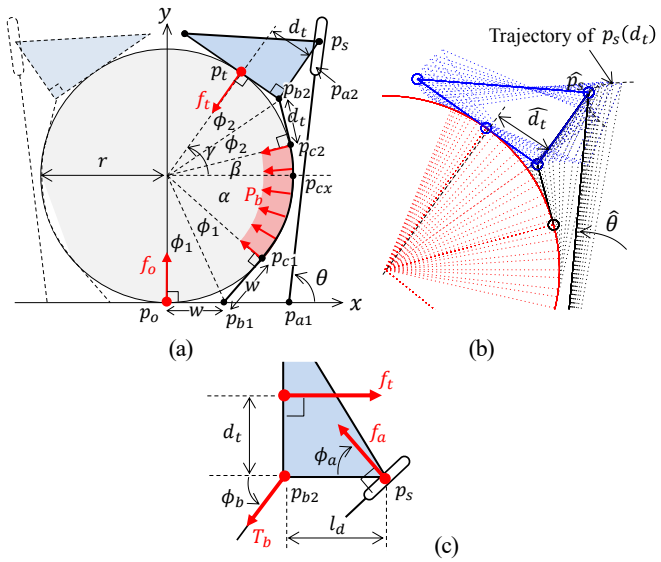

Fig. 5. (a) Pose of the finger grasping a circular object. (b) Equilibrium pose of the fingertip and the trajectory of p_s. (c) Free body diagram of the fingertip.

denote, the center point of the palm, the proximal and distal points of the belt, the proximal and distal points of the actuation link, and the contact point with an object at the fingertip, respectively. w, d_b, l_a, and l_t mean the distance between p_o and p_{b1}, the length of the belt, the length the actuation link, and length of the contact surface of the fingertip, respectively. The points p_{c1}, p_{c2}, and p_{cx} in Fig. 5(a) indicate the lower and upper border points of the contact area of the belt and the point at the horizontal line, respectively. The angles determined by the center of the object and the points p_o, p_{b1}, p_{c1}, p_{cx}, p_{c2}, p_{b2} and p_t are named as ϕ_1, α, β, and ϕ_2, respectively, and calculated as

$$\phi_1 = \text{atan}(w/r), \quad \phi_2 = \text{atan}(d_t/r),$$
$$\alpha = \pi/2 - 2\phi_1, \quad \beta = (d_b - w - r\alpha - d_t)/r.$$

For the convenience of calculation, let us define

$$\gamma \equiv \beta + 2\phi_2.$$

From these, the positions of p_t, p_{b2}, and p_s are calculated as follows:

$$p_t = [\, r\cos\gamma \;,\; r + r\sin\gamma \,]^T \tag{3}$$

$$p_{b2} = [r\cos\gamma + d_t\sin\gamma, r + r\sin\gamma - d_t\cos\gamma]^T \tag{4}$$

$$p_s = [\,(r + l_d)\cos\gamma + d_t\sin\gamma, r + (r + l_d)\sin\gamma - d_t\cos\gamma]^T \tag{5}$$

From (5), the actuation angle θ shown in Fig. 5(a) can be represented as

$$\theta(d_t) = \text{atan}\left(\frac{p_{sy}}{p_{sx} - w - l_d}\right) \tag{6}$$

where p_{sx} and p_{sy} are x and y elements of the p_s respectively. Note that the positions (3), (4), and (5) and the angle (6) are functions of d_t. By solving the following optimization problem, the equilibrium point of d_t can be found.

$$\max_{d_t \in [0, l_t]} \theta(d_t). \tag{7}$$

Fig. 5(b) illustrates all the possible fingertip poses satisfying $d_t \in [0, l_t]$ (dotted lines) and the equilibrium pose (solid lines). The trajectory of p_s according to d_t represented by a dotted black curve has a convex shape, which confirms that the equilibrium pose can be fully determined by kinematic information. In order to guarantee the grasping stability, two facts should be satisfied. First, the contact should be in the fingertip surface, i.e. $d_t \in [0, l_t]$. Second, contact forces and pressure should have positive values. The following subsection explains these.

B. Force Distribution at the Compliant Grasping Pose

Unlike other compliant grippers, the force and pressure distribution of the proposed gripper can be clearly formulated as it has a simple structure using the belt for uniform pressure distribution. Fig. 5(c) illustrates the free body diagram of the fingertip, where f_a and T_b mean the force from the actuation link and the belt tension respectively. The angles of the force vectors of f_a and T_b are

$$\phi_a = \gamma - \theta + \frac{\pi}{2}, \quad \phi_b = \beta - \gamma + \frac{\pi}{2}. \tag{8}$$

From the torque τ_a applied to the actuation link, f_a can be obtained as follows:

$$f_a = \tau_a\sqrt{(p_{sx} - w - l_d)^2 + p_{sy}^2}\,. \tag{9}$$

As the moment equilibrium around p_{b2} is $f_t d_t = f_a l_d \sin\phi_a$, the fingertip force f_t is

$$f_t = \left(\frac{l_d \sin\phi_a}{d_t}\right) f_a. \tag{10}$$

It can be rewritten by a vector as follows:

$$\overrightarrow{f_t} = [-f_t\cos\gamma\,,\; -f_t\sin\gamma]^T. \tag{11}$$

From the force equilibrium $f_t = f_a\cos\phi_a + T_b\cos\phi_b$, the tension of the belt can be calculated as follows

$$T_b = \frac{f_t - f_a\cos\phi_a}{\cos\phi_b}. \tag{12}$$

As the belt tension and the pressure has relationship $T_b = rP_b$, the pressure P_b is

$$P_b = T_b/r. \tag{13}$$

The total force cause by the pressure of the belt can be easily calculated by integrating the pressure P_b from p_{c1} to p_{c2}. The resultant force vector is

$$\overrightarrow{f_b} = [-T_b(\sin\beta + \sin\alpha)\,,\; T_b(\cos\beta - \cos\alpha)]^T, \tag{14}$$

and the magnitude is

$$f_b = T_b\sqrt{(\sin\beta + \sin\alpha)^2 + (\cos\beta - \cos\alpha)^2}. \tag{15}$$

Finally, from (11) and (14), the contact force on the palm f_o can be calculated. Because the sum of all the y-direction elements of the forces f_t, f_b, and f_o should be zero and f_o has only y-direction force

$$f_o = f_t\sin\gamma + T_b(\cos\alpha - \cos\beta). \tag{16}$$

In conclusion, (11), (14), and (16) show the overall force and pressure distribution. Figs. 6(a)-(f) show the simulated force and pressure distribution for the several circular objects with the diameters 40 – 140 mm, where w, d_b, l_d, l_a, and l_t were set to 21.5, 80, 23, 80, and 40 mm considering the actual design, respectively. For small objects, as shown in Fig. 6(a), the belt pressure is the dominant grasping force which is desirable to deal with the object. In most cases, the force and pressure are well distributed and the gripper provides stable form closure compared to other cases briefly illustrated in Fig. (2). But, when grasping the 140mm diameter object, the palm

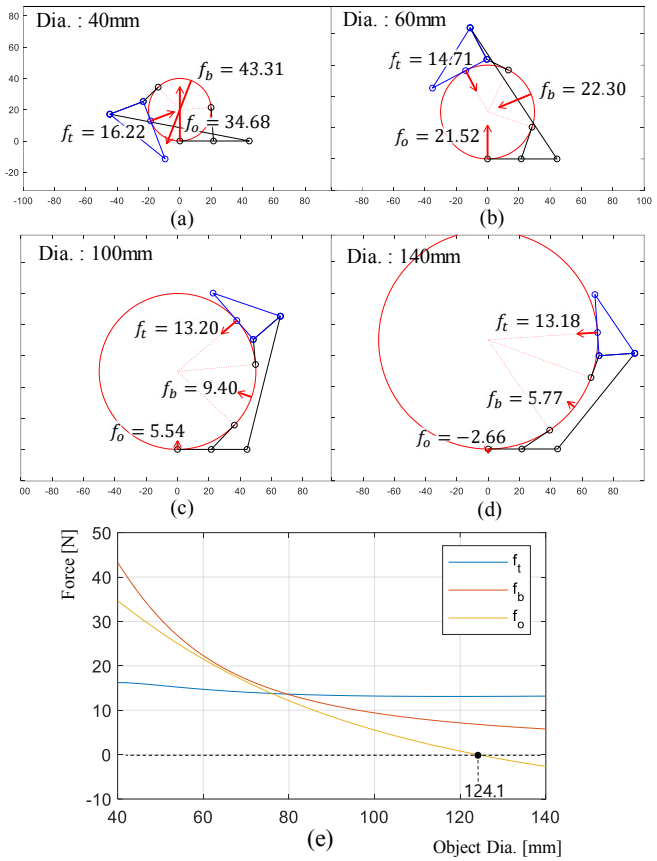

Fig. 6. (a)-(f) Force and pressure distribution for circular objects with the diameters 40, 60, 80, 100, 120 and 140 mm. (g) Force changes according to the object diameter.

contact force f_o becomes to negative value. Fig. 6(e) shows the changes of the forces according to the object diameter and it also shows that the palm loses contact force from a 124.1 diameter objects. This may not mean that it loses grasping stability. It can move to the different grasping mode with 2 contact areas, which will be analyzed in Subsection III.C. Another failure can occur when the contact point of the fingertip leaves the fingertip surface. but, in Fig. 6, the contact point resides almost at the center of the fingertip surface for all object sizes. This property is due to the shape of the slot. For instance, if the direction of the slot is inclined to one side, the contact point will move to the distal or proximal ends.

C. Two-Area Contact Case

When palm loses contact, only the fingertip force and the belt pressure grasp the object. Therefore, these two forces should be balanced in the y-direction. Considering the distance between the palm surface and the object, named d_o as shown in Fig. 7(a), θ, $\overrightarrow{f_t}$, $\overrightarrow{f_b}$ and f_o of (6), (11), (14) and (16) can be re-calculated. But these equations are functions of d_t as well as d_o. By solving the following constrained optimization, the feasible force and contact location can be obtained.

$$\max_{d_t,\, d_o} \theta(d_t, d_o) \qquad (17)$$

$$\text{subject to} \quad f_o = 0,\ 0 < d_t < l_t, \quad 0 < d_o.$$

Fig. 7(b) shows a simulation result about grasping a 126.4 mm diameter object. The contact area and the force from the belt

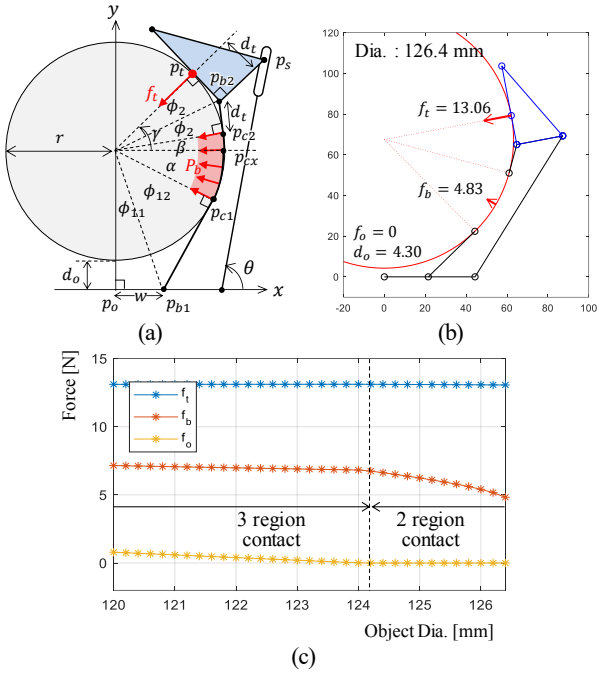

Fig. 7. (a) Pose of the finger in the case of two region contact ($f_o = 0$). (b) Simulation result for Dia. 126.4 mm object. (c) Closed up view of the force graph.

are small, and it is in the vicinity of the transition of grasping mode. The object bigger than about 127 mm diameter will be grasped by parallel pinching pose. Fig. 7(c) shows the close-up view of the force graph of Fig. 6.(e) considering 2 region contact. For the object with a diameter greater than 124.1 mm, palm contact force remains zero, and the belt force also decays to zero until grasping mode transit to the parallel pinching.

IV. Mechanical Design and Implementation

Fig. 8(a) shows the size and shape of the developed BLT gripper. It has 3-fingers and 5 motors. Each finger has one motor for flexion. To control the fingertip angle, a single motor placed at the palm frame adjusts the length of all the 3 belts. The last motor changes the orientation of the two side fingers simultaneously. Figs. 8(b)-(e) show various poses taken by actuating this orientation motor. If it rotates the fingers 180 deg as shown in Fig. 8(c), it can perform a parallel pinch or compliant grasp of cylindrical objects and also can perform a clasped pose. By completely folding the center finger and rotating the side fingers to 90 deg as shown in Fig. 8(e), 2-finger pinching is also available.

Fig. 9 illustrates the detail design of the finger and palm mechanisms. To increase holding force and save power, non-backdrivable worm gears were used for finger flexion as shown in Fig. 9(a). To achieve additional gear ratio, a spur gear set is used along with the worm gear. The motor for the belt actuation is placed at the palm frame as shown in Fig. 9(b). It actuates the 3 lead screws via a gear train and the sliders are connected to the lead screw nuts. For the finger rotation, the rotation motor placed at the palm frame delivers the motion through another gear train as shown in Fig. 9(c), which is a commonly used configuration for 3-finger grippers including BarrettHand™ [24][6][9]. Five identical 40 Watt ECX16 motors of MAXON Co. are used for actuation. The total

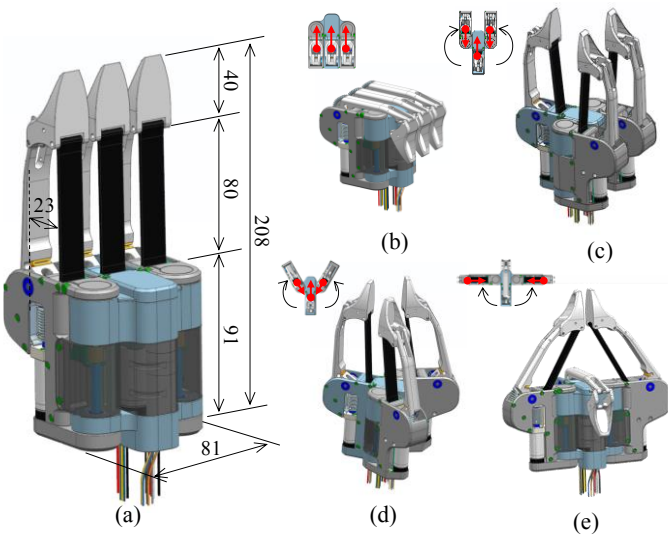

Fig. 8. (a) Size and shape of BLT gripper. (b) Clenched pose. (c) 3-finger 2-side parallel pinching. (d) 3-finger point symmetrical parallel pinching pose. (e) 2-finger parallel pinching.

weight is 1.2kg. A summary of specifications is presented in Table I.

V. Experimental Validation and Discussion

To verify the performance of the proposed gripper, grasping tests using various types of objects were conducted. Fig. 10 shows snapshots of the active and continuous transition from the precise parallel pinching mode to the compliant grasping mode, and again to the parallel pinching mode. The gripper picks up an 8 mm diameter pen by parallel pinching with the 3 fingertips as shown in Figs. 10(a) and (b). By actuating the belt motor with proper coordinated motions of the 3 flexion motors, the gripper moves the object to a proper position to be grasped (Fig. 10 (c)). Note that the contact point is distal to the critical line which means that the object is still in the parallel pinching region. This mode is desirable when adjusting the object position without being affected by compliant motions. By actuating the flexion motors, the object moves in the compliant grasping region and can be firmly grasped as shown in Figs. 10(d) and (e). By maintaining fixed fingertip angles, the opening of the fingers makes the object return to the parallel pinching region (Fig. 10(f)). Finally, by coordinate motions of the flexion motors and belt motors, the object returns to the parallel pinching pose as shown in Fig. 10 (g).

In order to prevent over-compression of the object when changing the fingertip angle (between Figs. 10(b) and (c)), the coordinated motions of the belt and the link are required. As illustrated in Fig. 11(a), the width of the object w_o from the centerline can be obtained as follows:

$$w_o = w + l_a \cos\theta_1 \tag{18}$$

where θ_1 is the flexion angle in the parallel pinching mode. By rotating the fingertip around a desired point p_r which is placed at the distal position from the contact points of the object (red-colored points in Figs. 11(a) and (b)), the fingertip angle can be safely changed without excessively squeezing the object. If the desired fingertip angle is ϕ_t, as can be seen in Fig. 11(b), the relationship between w_o and the required flexion

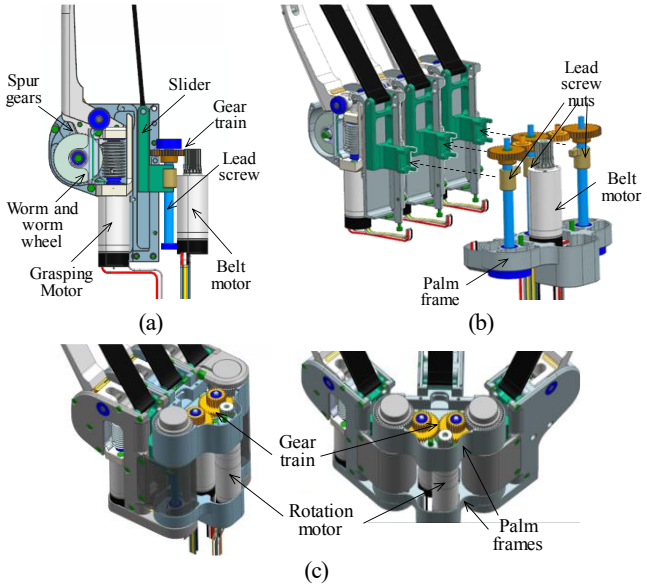

Fig. 9. (a) Finger flexion and slider mechanism. (b) Exploded view of the palm frame and the finger part. (c) Finer rotation mechanism.

Table I. Specification of BLT gripper

Size and weight	81 × 208 × 96 mm (W×H×T), 1.2 kg	
No. of actuators	Total 5 (Flexion 3, belt 1, rotation 1)	
Range of motion	Flexion	-30 ~ 90 deg
	Rotation	0 ~ 180 deg
	Fingertip[1)]	0~ 60 deg
Fingertip force	Peak force	60 N
	Holding force	60 N
	Cont. force	10 N
Gear ratio	Flexion	125 : 1
	Rotation	257.6 : 1
	Fingertip	172.7 : 1

1) Varies according to the finger pose

angle θ_2 is as follows:

$$w_o = w + l_d + l_a \cos\theta_2 - l_d \cos\phi_t - d_t \sin\phi_t$$

where d_t denotes the distance between p_r and p_{b2}. Thus,

$$\theta_2 = \text{acos}(w_o - w - l_d + l_d \cos\phi_t + d_t \sin\phi_t)/l_a. \tag{19}$$

From Fig. 11(b), the position of p_{b2} can be calculated as:

$$p_{b2} = \begin{bmatrix} x_{b2} \\ y_{b2} \end{bmatrix} = \begin{bmatrix} w + l_d + l_a \cos\theta_2 - l_d \cos\phi_t \\ l_a \sin\theta_2 - l_d \sin\phi_t \end{bmatrix}$$

Therefore, the required belt length d_{b2} to rotate the fingertip to ϕ_t is calculated as follows:

$$d_{b2} = \overline{p_{b1}p_{b2}} \tag{20}$$
$$= \sqrt{(l_d + l_a \cos\theta_2 - l_d \cos\phi_t)^2 + (l_a \sin\theta_2 - l_d \sin\phi_t)^2}$$

Consequently, by continuously actuating the flexion and belt actuators in accordance with (19) and (20), the fingertip angle can be safely changed without squeezing or damaging objects. On the other hand, as shown in Fig. 12, the BLT gripper also can directly perform the compliant grasping without going through the parallel pinching mode. By actuating flexion actuators with the fingertips inclined, the gripper can scoop the object to become the compliant grasping mode.

Fig. 13 shows several examples of grasping experiments of various types of objects. Figs. 13(a) and (b) show the grasping with the 3 fingers oriented symmetrically around the objects. The successful change in grasping mode is shown in these

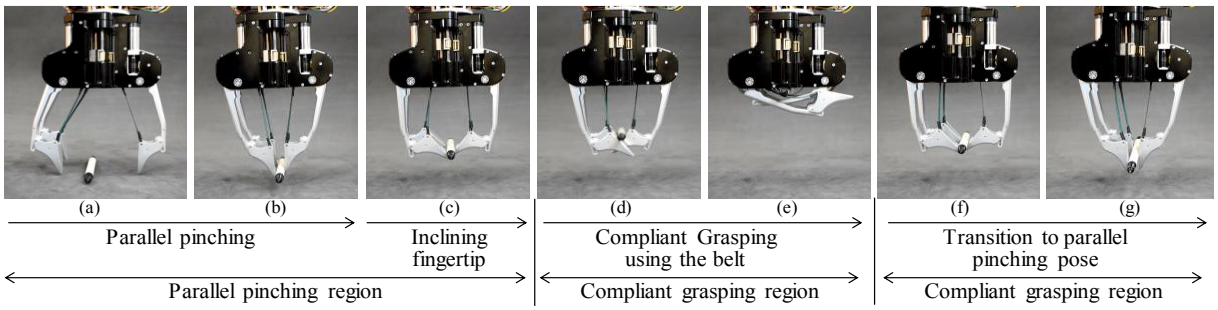

Fig. 10. Snapshots of active transition between precise parallel pinching and compliant grasping of a 8 mm diameter pen. After grasping, the gripper returns to the parallel pinching pose.

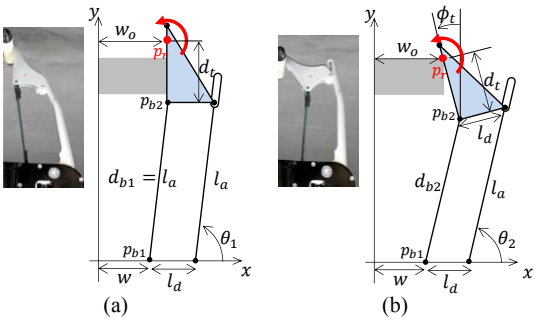

Fig. 11. Coordinated flexion and slider motions for the fingertip rotation to prevent squeezing the object with excessive force.

figures. In Fig. 13(c), the active transition of the grasping mode was unavailable because the fingertips are in contact with the middle of the flat surface of the object, and thus the fingertips cannot move under the object. It is a disadvantage compared to High-DOF dexterous hands which can perform in-hand manipulation using finger gaits. Figs. 13 (f)-(n) show snapshots from grasping experiments performed with various irregularly shaped objects. As can be found in Figs. 13(f) and (g), the motion allowed by the straight slot design enables the belts and fingertips to conform to the shape of the objects.

To observe the force and pressure distribution, pressure measurement was performed on several cylindrical objects. Fig. 14 (a) shows an experimental setup using Pliance Pressure Mat from Novel Co. Fig. 14(b) shows the pressure distribution on the center finger, where each cell is 2.5×2.5mm and the number in each cell represents the pressure in unit kPa. The results from grasping the 40 and 60 mm diameter objects show that the belt provides wide and even pressure distribution for the small objects as derived in Subsection III.B. When grasping the 80 mm diameter object, fingertip and palm forces take substantial contact force. In the case of the 100 mm diameter object, the fingertip force becomes dominant, which implies that it is near the verge of the parallel pinching mode. Due to the limited accuracy of the pressure mat, exact comparisons with the theoretical values were not performed. For the verification of precision, a repeatability test of the fingertip motion was performed. As shown in Fig. 14(c), 30 iterations of fingertip distance were measured and the maximum deviation from the average distance was 0.0321 mm. This precision is accomplished by the sufficiently large parallel 4-bar structures and flexible belt materials with high-stiffness.

The BLT gripper aims to achieve grasping mode adjustment,

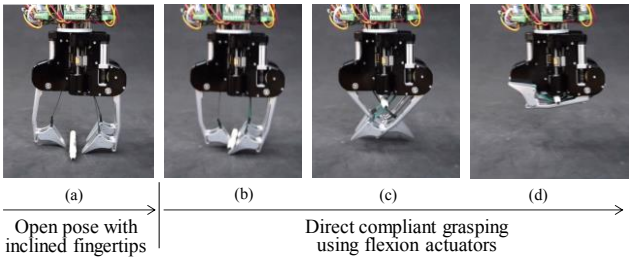

Fig. 12. Snapshots of direct compliant grasping of the 8 mm diameter pen without mode transition.

a goal that has also been studied with the iHY hand the Velo gripper. The iHY hand has 3 fingers and 5 actuators like the BLT gripper [9]. Each finger has one flexor tendon to achieve under-actuation. The fourth actuator controls the coupled rotational motion of two fingers, similar to the BLT gripper. To increase the manipulation capability, an additional extension tendon actuated by the fifth actuator was added to one finger of the iHY Hand. In contrast, the BLT gripper utilizes one actuator to adjust all three fingertip angles simultaneously to achieve active grasping mode change while maintaining the parallel 4-bar structure for precision. It is notable that iHY hand has flexure joints instead of revolute joints. This enables remarkable robustness against collisions at the expense of a certain level of precision, which is a clear difference from the design philosophy of the BLT gripper. The Velo gripper also has both capabilities of the parallel pinching and compliant grasping [17]. To maintain the parallel finger angles, coupling tendons instead of the parallel 4-bars were used. It can be advantageous for a wide range of motion but the precision can be lower than the 4-bar mechanism. The grasping mode of the Velo gripper is also determined by the contact point with objects, while the BLT gripper can actively change the mode by using one more actuator. Another difference between the BLT gripper and these other grippers is that the contact occurs on a surface of the belt in tension with uniform pressure not concentrated on a point or line. This is a desirable property for compliant grasping.

VI. Conclusion and Future Work

This paper presented a 3-finger 5-DOF adaptive gripper that has active transition capability between the precise parallel pinch and compliant grasp. The simple and unique finger mechanism provides an appropriate grasping pose with stable form closures and applies well-distributed grasping force and pressure to the objects with the arbitrary size. The gripper

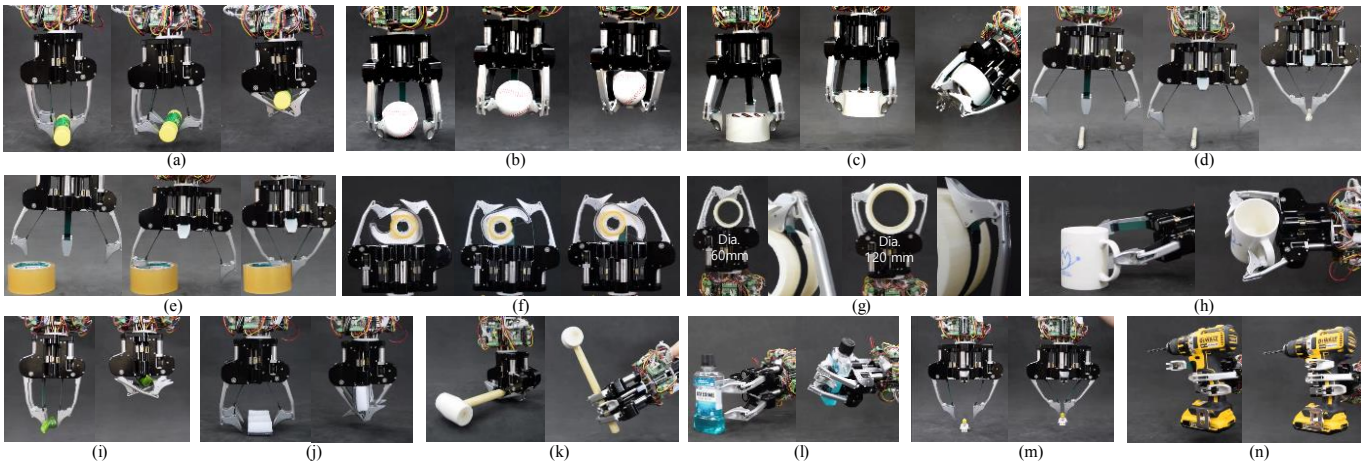

Fig. 13. (a) and (b) Active transition with cylindrical and spherical objects. (c) Pinching and grasping of a cylindrical object where the grasping mode was manually changed. (d) and (e) 2-finger parallel pinching. (f)-(m) grasping irregular shaped and various sided objects. (n) grasping and operating a hand drill.

mechanism was carefully designed with the consideration of practical applications and future commercialization; using the minimum number of the actuators maintaining enough capability of various grasping tasks, achieving high payload and durability, and active transition of the grasping mode without complicated control algorithm. The force and pressure analysis and the experimental results verified the grasping performance and active transition capability.

For the future work, robust and reliable joint torque sensors and fingertip force sensors will be developed. Improvement including additional weight and size minimization will be carried out with the aim of being widely used as a versatile tool to accelerate the progress in field of robot manipulation.

REFERENCES

[1] M. Cutkosky, "On grasp choice, grasp models, and the design of hands for manufacturing tasks," IEEE Trans. on Robotics and Automation, Vol. 5, No. 3, pp. 269–279, 1989.

[2] T. Feix, et al., "The grasp taxonomy of human grasp types," *IEEE Trans. on Human–Machine Systems*, Vol. 46, No. 1, pp. 66–77. 2016.

[3] M. Grebenstein, et al., "Antagonistically driven finger design for the anthropomorphic DLR Hand Arm System," *IEEE Int. Conf. on Intelligent Robots and Systems*, pp. 1836 - 1842, 2011.

[4] https://www.shadowrobot.com/products/dexterous-hand/

[5] Y.-J. Kim, et al., "Fluid Lubricated Dexterous Finger Mechanism for Human-Like Impact Absorbing Capability," *IEEE Robotics and Automation Letters*, Vol. 4, No. 4, pp. 3971-3978, Oct. 2019.

[6] T. Laliberte, et al., "Underactuation in robotic grasping hands," Machine Intelligence & Robotic Control, vol. 4, no. 3, pp. 1-11, 2002.

[7] Cosimo, et al., "Toward Dexterous Manipulation with augmented adaptive synergies: the Pisa/IIT SoftHand 2," *IEEE Trans. on Robotics*, Vol 34, No 5, Oct. 2018.

[8] R. Deimel, et al., "A novel type of compliant and underactuated robotic hand for dexterous grasping," *International Journal of Robotics Research,* Vol. 35, No. 1, August 2015.

[9] L. U. Odhner, et al., "A compliant, underactuated hand for robust manipulation," *The International Journal of Robotics Research*, vol. 33, pp. 736-752, 2014.

[10] R. Ma and A. Dollar, "Yale OpenHand Project: Optimizing Open-Source Hand Designs for Ease of Fabrication and Adoption," *IEEE Robotics & Automation Magazine*, vol. 24, pp. 32-40, 2017.

[11] N. C. Dafle, et al., "Extrinsic Dexterity: In-Hand Manipulation with External Forces," *IEEE Int. Conf. on Robotics & Automation (ICRA)*, pp. 1578-1585, May 2014.

[12] L. Ddhner, et al., "Precision Grasping and Manipulation of Small Objects from Flat Surfaces using Underactuated Fingers," *IEEE Int. Conf. on Robotics & Automation (ICRA)*, pp. 2830-2835, May 2012.

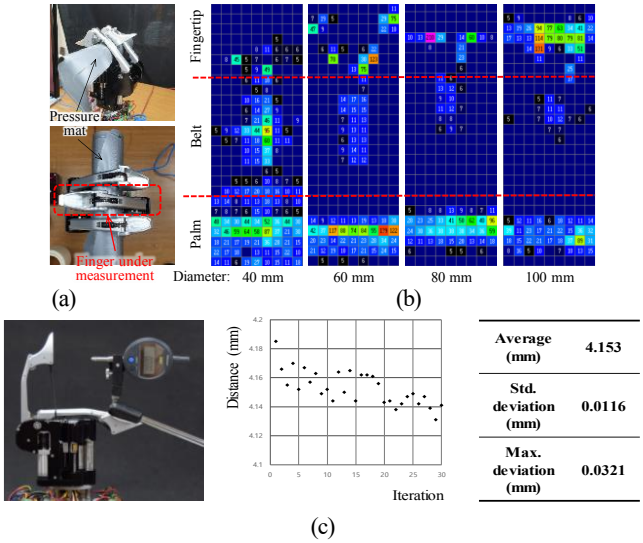

Fig. 14. Measurement of the pressure for cylindrical object grasping. (a) Experimental setup (Pliance Pressure Mat, Novel Co.). (b) Measured data for diameters 40, 60, 80, and 100 mm (Cell size: 2.5 mm^2 , unit: KPa). (c) Repeatability test using a dial gauge (Mitutoyo Co. resolution 0.001 mm).

[13] V. Tincani, et al., "Implementation and control of the Velvet Fingers: A dexterous gripper with active surfaces," *IEEE Int. Conf. on Robotics and Automation*, pp. 2744-2750, 2013.

[14] M. Ciocarlie, et al., "The Velo gripper: A versatile single-actuator design for enveloping, parallel and fingertip grasps*," The International Journal of Robotics Research*, vol. 33, pp. 753-767, 2014.

[15] https://robotiq.com/products/3-finger-adaptive-robot-gripper

[16] US20140265401A1, US Patent, 2014.

[17] T. Nishimura, et al., "Variable-Grasping-Mode Underactuated Soft Gripper With Environmental Contact-Based Operation," *IEEE Robotics and Automation Letters*, vol. 2, no. 2, pp. 1164-1171, April 2017.

[18] H. Liu, et al., "Modeling, Optimization, and Experimentation of the ParaGripper for In-Hand Manipulation Without Parasitic Rotation," *IEEE Robotics and Automation Letters*, vol. 5, pp. 3011-3018, 2020.

[19] L-W Tsai, *Robot Analysis*, John Wiley & Sons, Inc., 1999, pp. 339-350.

[20] https://www.festo.com/cms/en_corp/9779_10391.htm#id_10391

[21] S. Kim, et al., "Smooth Vertical Surface Climbing With Directional Adhesion," *IEEE Trans. On Robotics*, Vol. 24, No.1 Feb., 2008.

[22] Y. Lee, et al., "Flexible sliding frame for gait enhancing mechatronic system (GEMS)," *Int. Conf. of the IEEE Engineering in Medicine and Biology Society (EMBC)*, pp. 598-602, 2016.

[23] Y-J Kim, et al., "Development of a soft robotic glove with high gripping force using force distributing compliant structures," *IEEE/RSJ Int. Conf. on Intelligent Robots and Systems (IROS)*, pp. 3883-3890, Sept. 2017.

[24] https://advanced.barrett.com/barretthand